Properties of the δ Scorpii Circumstellar Disk from Continuum Modeling

A. C. Carciofi[1], A. S. Miroshnichenko[2,3], A. V. Kusakin[4,5], J. E. Bjorkman[3], K. S. Bjorkman[3], F. Marang[6], K. S. Kuratov[5], P. García-Lario[7], J. V. Perea Calderón[8], J. Fabregat[9] and A. M. Magalhães[1]

carciofi@usp.br

ABSTRACT

We present optical $WBVR$ and infrared $JHKL$ photometric observations of the Be binary system δ Sco, obtained in 2000–2005, mid-infrared (10 and 18 μm) photometry and optical ($\lambda\lambda$ 3200–10500 Å) spectropolarimetry obtained in 2001. Our optical photometry confirms the results of much more frequent visual monitoring of δ Sco. In 2005, we detected a significant decrease in the object's brightness, both in optical and near-infrared brightness, which is associated with a continuous rise in the hydrogen line strenghts. We discuss possible causes for this phenomenon, which is difficult to explain in view of current models of Be star disks. The 2001 spectral energy distribution and polarization are succesfully modeled with a three-dimensional non-LTE Monte Carlo code which

[1]Instituto de Astronomia, Geofísica e Ciências Atmosféricas, Universidade de São Paulo, Rua do Matão 1226, Cidade Universitária, São Paulo, SP, 05508–900, Brazil

[2]Department of Physics and Astronomy, University of North Carolina at Greensboro, P.O. Box 26170, Greensboro, NC 27402–6170, USA

[3]Ritter Observatory, Department of Physics and Astronomy, University of Toledo, Toledo, OH 43606–3390, USA

[4]Sternberg Astronomical Institute, Universitetskij pr. 13, Moscow, Russia

[5]Fesenkov Astrophysical Institute, Kamenskoe plato, Almaty 480068, Kazakhstan

[6]South African Astronomical Observatory, PO Box 9, Observatory 7935, South Africa

[7]European Space Astronomy Centre, Research and Scientific Support Department of ESA, Villafranca del Castillo, Apartado de Correos 50727, E–28080 Madrid, Spain

[8]European Space Astronomy Centre, Villafranca del Castillo, Apartado de Correos 50727, E–28080 Madrid, Spain

[9]Observatorio Astronómico, Universidad de Valencia, 46100 Burjassot, Spain

produces a self-consistent determination of the hydrogen level populations, electron temperature, and gas density for hot star disks. Our disk model is hydrostatically supported in the vertical direction and radially controlled by viscosity. Such a disk model has, essentially, only two free parameters, viz., the equatorial mass loss rate and the disk outer radius. We find that the primary companion is surrounded by a small (7 $R_\star$), geometrically-thin disk, which is highly non-isothermal and fully ionized. Our model requires an average equatorial mass loss rate of $1.5 \times 10^{-9} M_\odot$ yr^{-1}.

Subject headings: techniques: photometric, polarimetric; methods: numerical; stars: emission-line, Be; stars: individual (δ Scorpii); circumstellar matter

1. Introduction

Line emission in most stellar spectra arises from ionized gas beyond the photospheric level. In particular, emission-line spectra of B-type stars (e.g., Be, B[e], Herbig Ae/Be) are due to extended circumstellar (CS) envelopes. Additionally, the ionized CS gas produces continuum radiation due to free-free and free-bound transitions (Gehrz, Hackwell, & Jones 1974). The envelope contribution to the object's brightness depends on the distribution of the density, temperature, and ionization degree throughout the envelope.

Classical Be stars are a large class of objects in which CS contribution to the stellar continuum can be significant. These variable non-supergiant stars were found to show transitions between active (with line emission) and passive (or diskless, without line emission) phases (Porter & Rivinius 2003). In their active phase, Be stars exhibit moderately strong emission-line spectra (equivalent width of the Hα line can be up to $\sim$70 Å) and display large IR excesses, which can be up to $\sim$40 times larger than the photospheric flux of the central star at 12μm (Beichman et al. 1988). It has also been shown that the Hα line strength correlates with the IR excess (Chokshi & Cohen 1988).

Given the high level of the IR CS continuum, a question of the importance of the CS contribution to the optical continuum arises. It is definitely lower than in the IR, since photospheric lines are seen in the optical range and the observed optical color-indices are not far from intrinsic ones. However, the effect of the envelope parameters on the CS continuum has not been studied in any significant detail. If the optical excess radiation is large, it may affect at least the determination of the Be star luminosities and the amount of their CS gas as well as parameters derived from the line profile modeling. From a comparison with normal B-type dwarfs and giants, Zorec & Briot (1991) showed that the optical CS excess radiation

can be as large as 1 mag and that it also correlates with the Balmer line strength. This study used pre-Hipparcos distance determinations and average V-band brightnesses that could have affected the derived CS luminosity excesses, but it qualitatively demonstrated the importance of the optical CS emission to the total flux.

Although optical photometric observations of Be stars are counted in tens of thousands (e.g., Pavlovski et al. 1997; Percy & Bakos 2001), simultaneous photometric and spectral observations are still rare, and only a few Be stars have been observed in both phases (active and diskless) with both techniques. These data show, for example, that the optical brightness of γ Cassiopeae was about 0.7 mag fainter in a diskless phase than in an active phase with the strongest Hα emission (see Hummel 1998). Observations of π Aquarii, which had the most active phase in late 1980's and has lost the line emission completely in 1996, show that the V-band brightness difference between the two phases was $\sim$0.5 mag (Bjorkman et al. 2002). This study has shown that, in the diskless phase, π Aqu has lost its entire IR excess, indicating that the CS gas has vanished from the system.

In the summer of 2000, one of the brightest B-type stars, δ Scorpii, exhibited first signs of line emission. Follow-up photometric and spectroscopic monitoring (Gandet et al. 2002; Miroshnichenko et al. 2003) showed that the primary companion of this binary system had a steadily developing CS disk. In particular, the system became $\sim$0.7 mag brighter in the V-band. Its Hα strength increased with time, and an initially double-peaked line profile became single-peaked in 2003 (Miroshnichenko et al. 2003).

Line profiles in Be stars are still ambiguously interpreted by different models (e.g., Hummel & Vrancken 2000; Chesneau et al. 2005). Therefore, it is important to constrain CS parameters using photometric observations. Unfortunately, only a few photoelectric photometric observations of δ Sco in more than one band have been published so far (Gandet et al. 2002).

This paper has two main goals. In § 2 we present multiwavelength photoelectric photometry of δ Sco obtained in 2000–2005, and in § 3 we present a detailed modeling of the CS disk of δ Sco using the 2001 spectral energy distribution (SED) and polarization. In §§ 4–5 we discuss our results and present our conclusions.

2. Observations

The photometric $WBVR$ observations of δ Sco were obtained in 2002–2005 at the Tien-Shan Observatory (TSAO, Kazakhstan) with a 50-cm telescope and a standard pulse-counting single-channel photometer. The instrumental system, whose BVR bands are very

close to the Johnson system and W-band is a shorter version of the Johnson U-band, is described in Khaliullin et al. (1985). The $W-B$ color-indices were transformed to the wider used $U-B$ using the following relationship for early B-type dwarfs (B0–B3) that is based on comparison of the Johnson photometry and data from the original $WBVR$ catalog of Kornilov et al. (1991): $U-B=(0.83\pm0.01)\,(W-B)+(0.04\pm0.01)$.

The Johnson $BVRIJHK$ observations were obtained in 2002 at the 1 m TSAO with the 2-channel photometer-polarimeter FP3U of the Pulkovo Observatory (Bergner et al. 1988). The errors of individual measurements do not exceed 0.03 mag in all the bands. HR 5984 (B0.5 V) and HR 5993 (B1 V) were used as comparison stars at both TSAO telescopes. Stability of the instrumental system was controlled using other standard stars observed during the night.

In 2000–2005 we obtained JHK photometry of δ Sco at the 1.55-m Carlos Sánchez Telescope (CST), operated by the Instituto de Astrofísica de Canarias at the Spanish Observatorio del Teide (Tenerife, Spain). We used a CVF infrared spectrophotometer equipped with an InSb photovoltaic detector, operating at the temperature of liquid nitrogen, with a photometric aperture of $15''$ and a chopper throw of $30''$ in the E-W direction to subtract the contribution from the background sky. The Teide photometric system, as well as its relations with other standard photometric systems, is described in Arribas & Martínez-Roger (1987). The JHK photometry in 2005 was obtained with the photometer FIN that replaced the CVS at the CST. FIN is also equipped with a liquid nitrogen cooled InSb detector and works in chopping mode. The aperture and chopper throw were $15''$ and $25''$, respectively. The measurement uncertainties does not exceed 0.03 mag in all the bands.

Additional $JHKL$ photometric data were obtained at the 0.75–meter telescope of the South-African Astronomical Observatory equipped with a single–element InSb photometer and calibrated with the SAAO photometric system (Carter 1990). The optical (V-band) and near-IR (K-band) light curves along with the amateur visual brightness estimates are shown in Figure 1.

The IR imaging was performed on October 22, 2001, at Mauna Kea with the 3 m NASA Infrared Telescope Facility (IRTF) and the IR camera MIRLIN. The camera has a 128×128 pixel, high-flux Si:AS BIB detector with a plate scale of $0\farcs475$ at IRTF. Background subtraction was carried out by chopping the secondary mirror at an 11 Hz rate with a $15''$ throw in the north-south direction and by nodding the telescope a similar distance in the east-west direction. The observations were obtained in the N (effective wavelength $\lambda_{\rm eff}$=10.79 μm and passband $\Delta\lambda$=5.66 μm) and Q_s ($\lambda_{\rm eff}$=17.90 μm and $\Delta\lambda$=2.00 μm) bands. Five cycles, each consisting of 25 co-added 50 chop pairs, were carried out in the N band. In the Q_s band we also took 5 cycles, each containing 20 co-added 100 chop pairs. The closest

standard star, HR 6147, was observed 20 minutes after δ Sco, but at a higher elevation that caused a relatively large uncertainties in the measured brightness.

The imaging data were reduced using an IDL package developed at Jet Propulsion Laboratory (Pasadena) for MIRLIN. The resultant image has a 32×32 pixel field. The total flux within the object's images was measured using the PHOT task under the APPHOT package in IRAF. The object's brightness was calibrated using known brightness of the standard stars in the N ($\lambda_{\rm eff}$=10.8 μm, $\Delta\lambda$=5.6 μm) and Q_s ($\lambda_{\rm eff}$=17.9 μm, $\Delta\lambda$=1.7 μm) bands and in the IRAS 12 and 25 μm bands. The IRTF photometric system is defined in Hammersley et al. (1998). The brightness of δ Sco turned out to be 0.42±0.10 mag in N band and 0.9±0.2 mag in Q_s band.

Optical spectropolarimetry was obtained in April-July 2001 using the half-wave polarimeter (HPOL) at the 0.9 m telescope of the University of Wisconsin's Pine Bluff Observatory (PBO). For details about the observing program, instrument, and data reduction, see Wolff, Nordsieck, & Nook (1996) and references therein. Observations were made successively in two separate spectral ranges: blue (3190–6050 Å) and red (5960–10410 Å).

3. Modeling

δ Sco has been a standard for spectral classification (spectral type B0 IV) since long ago. Its photometric properties have also been measured at different epochs and showed no obvious variations (see Miroshnichenko et al. 2001, for more information). The object is a non-eclipsing binary system with a ∼1.5 mag optically fainter secondary companion with an orbital period of 10.6 years (Bedding 1993) and a highly eccentric orbit (e=0.94, Miroshnichenko et al. 2001). In order to determine the object's SED before the beginning of the Be phase, we collected available optical and IR photometric data from the literature. These include optical and near-IR photometry in the region 0.3–4.8μm (Thé et al. 1986) and IRAS data at 12 and 25μm (Beichman et al. 1988). Inspection of the resulting SED shows no deviation from the theoretical SED (Kurucz 1994) for the primary's parameters from Table 3. This indicates that the secondary's $T_{\rm eff}$ is not significantly different from that of the primary. Therefore, we simply removed 15% of the dereddened flux at all the wavelengths to construct the pre-active (diskless) phase SED of the primary, shown as the asterisks in Figure 2.

We now have to choose an SED that is representative of the active phase. The light curve of δ Sco in 2001–2004 is characterized by a somewhat well-defined plateau around $V \approx 1.7$ mag, with several short fadings (timescales of weeks to months, Figure 1). As will

be discussed more fully in § 4, these variations are probably a result of a modification of the properties of CS disk, perhaps an increase of the mass loss rate associated with a change in the geometry. We assume that the fadings are transient perturbations of a more static disk configuration which is associated with the $V = 1.7$ mag plateau, and is represented by a somewhat smooth density distribution of the CS gas. We, therefore, construct the active phase SED from the highest fluxes obtained by us. The active-phase SED is shown as the filled circles in Figure 2.

3.1. Disk Model

Observational evidence supports the idea that the disks of classical Be stars are Keplerian (rotationally supported) gaseous disks (see Porter & Rivinius 2003, for a recent review). The essential physics that determines the geometrical structure of Keplerian disks is reasonably well understood. The disk radial structure is governed by viscosity (Lee, Saio, & Osaki 1991), while the vertical structure is controlled by gas pressure.

Assuming a steady-state isothermal outflow, the disk density structure is given, in cylindrical coordinates (ϖ, z, ϕ), by

$$\rho(\varpi, z) = \frac{\Sigma(\varpi)}{\sqrt{2\pi}H(\varpi)} \exp\left(-\frac{z^2}{2H^2}\right). \tag{1}$$

(see, for example, Bjorkman 1997). Using the viscosity prescription of Shakura & Sunyaev (1973), the disk surface density, Σ, is given by

$$\Sigma(\varpi) = \frac{\dot{M} v_{\rm crit} R_\star^{1/2}}{3\pi\alpha a^2 \varpi^{3/2}} \left(\sqrt{R_d/\varpi} - 1\right), \tag{2}$$

where α is the viscosity parameter. The density scale is controlled primarily by the equatorial mass loss rate, $\dot{M}$, but also by the critical rotational velocity of the star, $v_{\rm crit}$, and the disk temperature via the sound speed, a. For isothermal disks with large R_d, the surface density is a power-law function of the radial distance, $\Sigma \propto \varpi^{-2}$.

The disk scale-height, H, is given by

$$H(\varpi) = (a/v_\phi)\varpi. \tag{3}$$

Since the disk is isothermal and the ϕ component of the velocity is Keplerian ($v_\phi = v_{\rm crit}\varpi^{-1/2}$), we find the familiar result that an isothermal disk flares as $H \propto \varpi^{1.5}$. It follows from Eqs. (1) and (3) that, for isothermal disks, the density falls very sharply with radius as $\rho \propto \varpi^{-3.5}$. Another important property of Keplerian disks can be readily derived from Eq. (3). Since

v_ϕ is much larger than the sound speed (the first is of the order of several hundreds of km/s and the second a few tens of km/s), the disk scaleheight is small compared to the stellar radius and the disk is geometrically thin.

To conclude this brief description of the properties of isothermal Keplerian viscous disks, we must describe their velocity structure. The ϕ component is Keplerian, as stated above, but those disks must have an outflow velocity, which is given by the mass conservation relation

$$v_\varpi = \frac{\dot{M}}{2\pi\varpi\Sigma} \, . \tag{4}$$

Recently, Carciofi & Bjorkman (2006, hereafter CB) presented a new three-dimensional non-LTE Monte Carlo (MC) code for solving the radiation transfer and radiative equilibrium problem for arbitrary gas density and velocity distributions. The code was used to study the thermal properties of the disks around classical Be stars.

CB found that the optically thick part of Be star disks are highly non-isothermal, with kinetic temperature ranging from about 30% of the stellar effective temperature ($T_{\rm eff}$) in the midplane to temperatures close to $T_{\rm eff}$ near the stellar surface. CB also found that the disks are generally fully ionized, but for later spectral types (B5 and later) the midplane can become neutral, depending on the disk density scale.

From Eqs. (1) to (3), it is evident that the temperature plays an important role (via de sound speed) in the disk density structure; therefore, a self-consistent solution for the disk density, that takes into account all the non-LTE and three-dimensional radiative transfer effects on the disk temperature, is required to accurately predict the properties of the CS disk. This was done by Carciofi et al. (2006) who built upon the previous code and presented a self-consistent solution for the disk density (see also Bjorkman & Carciofi 2005). Given a prescription for the viscosity (e.g., Shakura & Sunyaev 1973) the disk model has only two free parameters, the disk mass loss rate and outer radius. All other quantities (surface density, vertical density and outflow speed) are determined self-consistently from the solution of the fluid equations. In this paper, we use an updated version of the CB code to model the active-phase SED and polarization of the primary companion of δ Sco.

3.2. Best-fitting Model

The parameters of the primary companion were taken from Miroshnichenko et al. (2001) and are summarized in Table 3. We assume that the disk around the primary companion is in the orbital plane of the binary system, so the disk inclination angle is the same as the

orbital inclination angle i, and is a fixed parameter in our modeling within the observationally derived error of $\pm$ 5°. Also, we assume a value of 0.1 for the viscosity parameter of Shakura & Sunyaev (1973).

Figure 2 shows our best-fitting SED along with the observed data. We see that our model reproduces well the observed SED for all wavelengths. Our best-fitting model consists of a very dense (midplane density at the stellar surface, ρ_0, of $4.5 \times 10^{-10}\,\mathrm{g\,cm^{-3}}$) but small ($R_d = 7R_\star$) disk. In § 3.3 we discuss in more detail the properties of our solution for the disk. The parameters of our best-fitting model are listed in Table 4.

There is a number of interesting points to consider in Figure 2. From the J-band longward ($\lambda > 1.25$ μm) the SED is completely dominated by the disk emission and the stellar flux corresponds to only 1–20% of the total flux, depending on the wavelength. The stellar flux dominates the spectrum only for $\lambda \lesssim 4000$Å, but the disk emission still contributes at an important level down to $\lambda \sim 2000$Å.

Another interesting feature of the SED is that, in addition to the usual IR excess, there is a small UV excess just longward of the Lyman jump. This UV excess is a result of electron scattering in the disk, which redirects some of the stellar flux into the polar direction.

Finally, we call attention to the fact that the unprocessed stellar radiation (*dash-dot* line in Figure 2), which corresponds to the SED that the object would have without the disk, matches very well the pre-active SED. This is an important verification of our disk model, because it shows that it predicts correctly the excess flux emitted by the CS material.

The polarization results are shown in Figure 3. Because of the large error of the observed polarization in some wavelength regions, we bin the data so that the wavelength size of the bin changes to keep a constant polarization error of 0.01%. Even using this procedure, we still observe a large scatter in the data, which makes us believe that the actual errors in the bins may be larger.

The observed polarization was corrected for the interstellar contribution according to the measurement by Hall (1958). The later (B-band polarization degree of 0.3% and polarization angle of 118°) was most likely obtained in the early 1950's, during the diskless (i.e., intrinsically unpolarized) phase.

Since we do not include the secondary in our modeling, the model polarization (dotted line in Figure 3) must be changed in order to account for the unpolarized flux of the secondary. The depolarized curve is shown as the thick solid line of Figure 3.

We see that there is a general good agreement between the model and the observations. For the blue part of the Paschen continuum ($\lambda \lesssim 0.6\mu$m), both the shape and level of the

polarization are correct, but our model predicts a somewhat smaller polarization for the red part. Unfortunately, the observations were not able to resolve the Balmer jump, but they do resolve the Paschen jump at 0.82 μm and there is a rough agreement in the size of the jump. This is a particularly important result since the Paschen jump in polarization is controlled by the ratio of the $n = 3$ and $n = 4$ level populations, and the agreement between the model and the observations indicates that our non-LTE level populations are correct. Finally, we point out the good agreement of the polarization in the Brackett continuum ($\lambda > 0.82$ μm).

Let us now consider the uniqueness of our results for the disk parameters. For the case of dusty circumstellar shells, it is a well-known issue that fitting the SED alone can not well constrain the dust properties and spatial distribution (e.g., Carciofi, Bjorkman, & Magalhães 2004; Miroshnichenko et al. 1999). A similar issue is true here, because, as illustrated in Figure 4, there are several models that reproduce the observed SED equally well. For example, a larger and less dense disk ($R_d = 10\ R_\star$ and $\dot{M} = 7 \times 10^{-10}\ M_\odot\,\mathrm{yr}^{-1}$) is essentially equivalent to a smaller but denser disk ($R_d = 5\ R_\star$ and $\dot{M} = 2.5 \times 10^{-9}\ M_\odot\,\mathrm{yr}^{-1}$).

The linear polarization depends much more strongly on the model parameters ($\dot{M}$ and R_d) and, consequently, allows for breaking the degeneracy of the SED, as illustrated in Figure 5. The differences between the polarization levels of the three models shown are large enough to allow one to choose the 7 $R_\star$ model as to one that, for the most part, best reproduces the data.

3.3. Properties of the Solution

In this section we describe the properties of our solution for the structure of the disk of δ Sco. The temperature structure for our best fit model is shown in Figure 6. CB showed that the disks of Be stars are highly non-isothermal; indeed, in our results for δ Sco, the temperature goes from a minimum of 7000 K at the midplane, around $4R_\star$, to a maximum of about 30,000 K near the base of the disk.

As discussed in detail in CB, the temperature behavior is a mixture between that of optically thick disks of young stellar objects and optically thin winds of hot stars. For the optically thin upper layers of the disk (defined as the regions where the distance to the midplane is larger than one scaleheight), the temperature is nearly isothermal, with an average of about 0.6 $T_{\rm eff}$ or 16,000 K. At the midplane, however, the temperature has a complicated structure. At the base of the disk, the temperature is even larger than $T_{\rm eff}$ due to back-warming of the star. The temperature drops very quickly with radius and its profile is well-described by a flat blackbody reprocessing disk (Adams et al. 1987, see also CB for

more details).

In Figure 7 we show a map of the $n = 1$ hydrogen level population. We see that the disk is fully ionized, but there is a minimum in the ionization fraction ($\approx 90\%$) that coincides approximately with the minimum of the kinetic temperature. This ionization minimum occurs because of the deficit of photoionizing radiation due to the large optical depths of the midplane.

Following Carciofi et al. (2006), we use our solution for the disk temperature to self-consistently solve the fluid equations and determine the disk density. Let us analyze how our solution differs from the isothermal case of eqs. (1) and (3). In Figure 8 we show the disk opening angle as a function of radial distance, defined as

$$\theta = \tan^{-1}\left[\frac{H(\varpi)}{\varpi}\right]. \tag{5}$$

For reference we also show the opening angle of a corresponding isothermal disk with $\beta = 1.5$. As expected, the opening angles are very small and the entire disk is geometrically very thin. As a result of the small inclination angle of the system and the small vertical extent of the disk, the disk covers very little of the star and most of the hemisphere facing us is visible. This is one of the reasons why the polarization levels are small. In Figure 8 we see an interesting result: the opening angle is approximately constant in the inner disk, in striking contrast with isothermal disks that flare significantly. This result is explained by the rapid fall of the disk temperature with radial distance.

Let us, now, analyze the radial structure of the disk density, shown in Figure 9. We show, for comparison, the $\rho \propto \varpi^{-3.5}$ curve corresponding to the isothermal solution for the density. We see that the slope of the MC density profile for the inner part of the disk departs significantly from the -3.5 value; it is much less steep close to the star and is much steeper for $\varpi/R_\star \gtrsim 3$. This is, again, a result of the temperature structure in the midplane (see Carciofi et al. 2006, for detais).

4. Discussion

The disk model described above has only two free parameters: the equatorial mass loss rate and the disk size. All the macroscopic (density distribution, radial component of the gas velocity) and microscopic (hydrogen level populations and gas kinetic temperature) properties of the disk are self-consistently determined from those two parameters. Since the observables critically depend on the CS disk properties, both microscopic and macroscopic, it is of significance that our two-parameter model can successfully reproduce several different

observations of δ Sco.

The polarization, for instance, is critically dependent on two quantities: the geometry of the inner disk and the hydrogen level populations. We have seen above that the geometry of the inner disk is greatly altered by the temperature structure, with an interesting result that the inner disk is essentially unflared. Another quantity that is critically dependent on the details of the solution is the slope of the IR SED, which depends on the radial density profile, as demonstrated by Waters (1986).

We believe that our model provides a good description of the *average properties* of the CS disk of δ Sco, which, according to our assumptions, are associated with the highest brightness levels of the system in 2001. As we discuss below, our model cannot explain the large optical fadings of δ Sco because a dynamical model, with a variable and possibly asymmetrical mass loss, is probably required.

Our optical photometric data show that visual estimates of the δ Sco brightness collected by amateurs (e.g., Gandet et al. 2002) are generally correct (Figure 1). This is important for future interpretation of the entire active phase of δ Sco with dynamical models, which can take advantage of the detailed optical light curve.

Our modeling shows that the CS disk of δ Sco, about 2 years after the beginning of its formation, can be described as typical for Be stars. The disk is geometrically thin in the vertical direction and optically thick near the mid-plane. At the same time, the optical light curve (Figure 1) shows that a large flux excess ($\Delta V \sim 0.7$ mag), due to continuum emission from the disk, was achieved very quickly, in about 2 years. This is not typical of Be stars, since previous monitorings of their active phase show that the optical brightness raises generally slower. It took π Aqr about 2 decades (Bjorkman et al. 2002) and even longer to γ Cas (Telting et al. 1993) to reach its highest optical brightness. Other important difference between the light curve of δ Sco and the historical light curves of other Be stars is that the latter shows a good correlation between the emission-line strength (mostly Hα) and the optical brightness, which is not observed for δ Sco (see below).

Another feature of the light curve of δ Sco is the presence of multiple optical fadings that last from weeks to months. A striking feature is the pronounced fading in 2005, both in the optical and near-IR wavelengths, that was accompanied by a continuing rise of the line emission[1] (see bottom panel of Figure 1). This is a very unusual feature since other well-observed Be stars do not exhibit significant fadings, unless it is a transition to a diskless

[1]The spectroscopic data have not been analyzed yet. Preliminary results can be found at http://www.astrosurf.org/buil/becat/dsco/dsco_evol.htm.

phase (like that in π Aqr).

Miroshnichenko et al. (2003) noted this anti-correlation between the visual and Hα fluxes in the earlier evolution of the δ Sco disk and suggested that it might be explained by episodes of an increased mass loss. Such matter ejections would produce an increase in the Hα line emission strength which, in turn, would be followed by fadings of the optical brightness due to an increase in the disk optical depth.

This explanation for the optical fadings, however, raises more questions than it answers. In a system such as δ Sco, part of the optical flux comes from the star itself and part from the CS disk, so there are basically two ways to reduce the optical brightness: 1) to block part of the stellar disk; or, 2) to reduce, via some mechanism, the disk emission.

Since δ Sco has a low inclination angle ($i \approx 35^\circ$) and the CS disk is (probably) geometrically very thin, this means that only about 10% of the stellar flux can be blocked by the CS material, supposing a completely opaque disk in the vertical direction. It follows that, if process 1, above, is responsible for the large (0.3 mag or more) fadings observed in δ Sco light curve, *the geometry of the system must be changed* to explain the large attenuation of starlight. A possibility would be a radiatively warped disk, as proposed by Porter (1998). Such a warp would, effectively, place material at higher latitudes and increase the area of the stellar disk that could be blocked by the CS material. Another possibility is to have material to be ejected from the star not at the midplane, but at high latitudes. This ejection should, however, be nearly continuous in the timescale of the optical fading (weeks or months), since we expect the material to fall into the disk in an orbital timescale, which is of the order of one to a few days.

If, on the contrary, process 2 above is responsible for the fadings, the implications are somewhat similar. In our model, material is injected into the disk at the equator and slowly diffuses outward; therefore, an increase in the mass loss rate would result in an increase of the optical recombination radiation. Thus, a modification of the geometry of the system is required in this case also, if one wants to explain the optical fadings associated with increased line fluxes observed for δ Sco.

We conclude, from this short phenomenological discussion, that our static model of the δ Sco CS disk cannot explain the optical fadings and their anticorrelation with the Hα line strengths. We suggest that a more complex model with a different CS geometry is required to do that. It must be emphasized that polarization is a very important constraint on the disk geometry, since changes in the geometry would, most likely, result in variations of the polarization angle. This quantity, therefore, is of importance for constraining future dynamical models of δ Sco.

Another result of our modeling is that we require a disk size of 7 $R_\star$. This small value makes sense in view of the recent formation of the disk. Miroshnichenko et al. (2003) estimated the disk size based on the Hα profile parameters, assuming both Keplerian rotation ($v_\phi \propto \varpi^{-1/2}$) and angular momentum conservation ($v_\phi \propto \varpi^{-1}$), and found a disk size of $8R_\star$ for the first case and $2.8R_\star$ for the second. These spectroscopic estimates (averaged from the published ones for the beginning of 2001 and beginning of 2003) are based on a static approach to circumstellar gaseous rings by Huang (1972). It is interesting to note that the estimate assuming Keplerian rotation is very similar to the value that comes from our modeling.

5. Conclusions

We have obtained multicolor photometric observations (2000–2005) along with the entire optical range spectropolarimetry (2001) of the binary Be star δ Sco. Using these data, we constructed the system's SED in the range 0.4–18 μm that roughly corresponds to the maximum observed brightness.

Our photometric data confirm the visual light curve of δ Sco that is being carefully observed by amateur astronomers (see Gandet et al. 2002). It also traced a deep fading of the object in 2005, almost all the way to its diskless phase brightness level. This phenomenon is observed along with a continuous increase of the object's emission-line spectrum that makes it highly unusual. Similar anti-correlations of the brightness and emission-line strength on a smaller time- and amplitude-scale have been observed several times in 2000–2003 (Miroshnichenko et al. 2003). We suggest that this phenomenon may be explained by a significant change both in the mass loss rate and in the CS disk geometry. Further frequent photometric, spectroscopic, and polarimetric observations all the way to 2011, when the next periastron will occur, are very important for understanding of the disk formation and evolution in this highly eccentric Be binary.

We also modeled the observed SED, simultaneously with the linear polarization, using a new three-dimensional non-LTE Monte Carlo radiation transfer code. This code assumes that the disk is hydrostatically supported in the vertical direction and that its radial structure is governed by viscosity. The disk temperature and density structure are solved self-consistently given only two input parameters for the disk: the equatorial mass loss rate, which is assumed constant, and the disk outer radius. The basic parameters of the primary's CS disk are shown in Table 4. We find that a mass loss rate of $1.5 \times 10^{-9} M_\odot$ yr^{-1} and a disk size of $7R_\star$ best reproduces the available data.

Our solution for the disk temperature structure shows that, as have already been demonstrated by CB, the disk is highly nonisothermal, with temperatures ranging from 30% of the stellar effective temperature at the midplane, a few stellar radii away from the star, to temperatures of the order of the stellar temperature at the base of the disk. We also find that the disk is completely ionized.

The complex temperature structure of the disk has important consequences on the disk density structure. We show that our solution for the disk density departs significantly from the isothermal solution. Most noticeably, we find that the inner disk is essentially unflared, in contrast with the large flaring expected for isothermal models. Also, we find that the radial density profile departs significantly from the simple $n = -3.5$ power-law predicted for isothermal models. Since the slope of the IR SED is mainly controlled by the radial density structure, we suggest that careful measurements of the IR SED, mainly in the near IR, may be used to map the disk density and test the predictions of our model.

The next step in our modeling, which is already in progress, is to include the synthesis of hydrogen line profiles. This new quantity, associated with the SED and polarization, will help further constrain the disk parameters.

A. C. C. and A. M. M. acknowledge support from the São Paulo State Funding Agency FAPESP (grants 01/12589-1 and 04/07707-3). A. C. C. and J. E. B. acknowledge support from NSF grants AST-9819928 and AST-0307686. A. S. M. and K. S. B. acknowledge support from NASA grant NAG5–8054 and thank the IRTF staff for their assistance during the observations. P .G. L. and J. V. P. C. acknowledge support from grant AYA-2003-09499 from the Spanish Ministerio de Ciencia y Tecnología. A. M. M. acknowledges support from CNPq. We thank the PBO observing team, and especially Marilyn Meade, Brian Babler, and Ken Nordsieck, for their invaluable assistance with obtaining, calibrating, and reducing the HPOL spectropolarimetric data. This research has made use of the SIMBAD database operated at CDS, Strasbourg, France.

REFERENCES

Adams, F. C., Lada, C. J., & Shu, F. H. 1987, ApJ, 312, 788

Arribas S., Martínez-Roger C., 1987, A&AS, 70, 303

Bedding T. R., 1993, AJ, 106, 768

Beichman, C. A., Neugebauer, G., Habing, H. J., Clegg, P. E., & Chester, T. J., 1988. IRAS Catalogs and Atlases. Version 2. Explanatory Supplement, NASA Ref. Publ. 1190, 1

Bergner Yu. K., Bondarenko S.L., Miroshnichenko A. S., Yudin R. V., Yutanov N. Yu., Moralev Yu. D., Schumacher A. V., 1988, Izvestia Glavn. Astron. Obs. v Pulkove, 205, 142

Bjorkman, J. E. 1997, Circumstellar Disks, in Stellar Atmospheres: Theory and Observations, ed. J. P. de Greve, R. Blomme, & H. Hensberge (New York: Springer)

Bjorkman K. S., Miroshnichenko A. S., McDavid D. A., Pogrosheva T. M., 2002, ApJ, 573, 812

Bjorkman, J. E., & Carciofi, A. C. 2005, ASP Conf. Ser. 337: The Nature and Evolution of Disks Around Hot Stars, 337, 75

Carciofi A. C., Bjorkman J. E., 2006, ApJ, 639, 1081 (CB)

Carciofi, A. C., Bjorkman, J. E., Miroshnichenko, A. S., Magalhães, A. M., & Bjorkman, K. S. 2006, ASP Conf. Ser.: Active OB-Stars: Laboratories for Stellar and Circumstellar Physics, in press (astro-ph/0603116)

Carciofi, A. C., Bjorkman J. E., Magalhães A. M., 2004, ApJ, 604, 238

Carter B.S., 1990, MNRAS, 242, 1

Chesneau O., Meilland A., Rivinius T., et al., 2005, A&A, 435, 275

Chokshi A., Cohen M., 1988, AJ, 94, 123

Gandet, T. L., Otero, S., Fraser, B., & West, J. D., 2002, IBVS 5352

Gehrz R.D., Hackwell J.A., Jones T.W., 1974, ApJ, 191, 675

Hall, J. S. 1958, Publications of the U.S. Naval Observatory Second Series, 17, 1

Hammersley, P.L., Jourdain de Muizon, M., Kessler, M. F., Bouchet, P., Joseph, R. D., Habing, H. J., Salama, A., & Metcalfe, L., 1998, A&AS, 128, 207

Huang, S.-S., 1972, ApJ, 171, 549

Hummel W., 1998, A&A, 330, 243

Hummel W., Vrancken M., 2000, A&A, 359, 1075

Khaliullin Kh., Mironov A. V., Moshkaliov V. G., 1985, Ap&SS, 111, 291

Kornilov V. G., Volkov I. M., Zakharov A. I., et al., 1991, Proceedings of the Sternberg Astron. Inst., v.63

Kurucz, R. L. 1994, Kurucz CD ROM 19, Solar Model Abundance Model Atmospheres, (Cambridge: Smithsonian Astrophysical Observatory)

Lee, U., Saio, H., & Osaki, Y. 1991, MNRAS, 250, 432

Miroshnichenko, A.S., Ivezić , Ž., Vinković , D., & Elitzur, M. 1999 ApJ, 520, L115

Miroshnichenko, A. S., Fabregat, J., Bjorkman K. S., et al., 2001, A&A, 377, 485

Miroshnichenko, A. S., Bjorkman K. S., Morrison N. D., et al., 2003, A&A, 408, 305

Pavlovski K., Harmanec P., Bozic H., Koubský P., Hadrava P., Kriiz S., Ruzic Z., Stefl S., 1997, A&AS, 125, 75

Percy J. R., Bakos A. G., 2001, PASP, 113, 748

Porter, J. M. 1998, A&A, 336, 966

Porter, J. M., & Rivinius, Th. 2003, PASP, 115, 1153

Shakura N. I., Sunyaev R. A., 1973, A&A, 24, 337

Sobolev V. V., 1960, Moving envelopes of stars, Cambridge: Harvard Univ. Press

Telting, J. H., Waters, L. B. F. M., Persy, J., & Dunlop, S.R. 1993, A&A, 270, 355

Thé P.S., Wesselius P.R., Janssen I.M.H.H., 1986, A&AS, 66, 63

Waters L. B. F. M., 1986, A&A, 162, 121

Wolff M. J., Nordsieck K. H., Nook M. A., 1996, AJ, 111, 856

Zorec J., Briot D., 1991, A&A, 245, 150

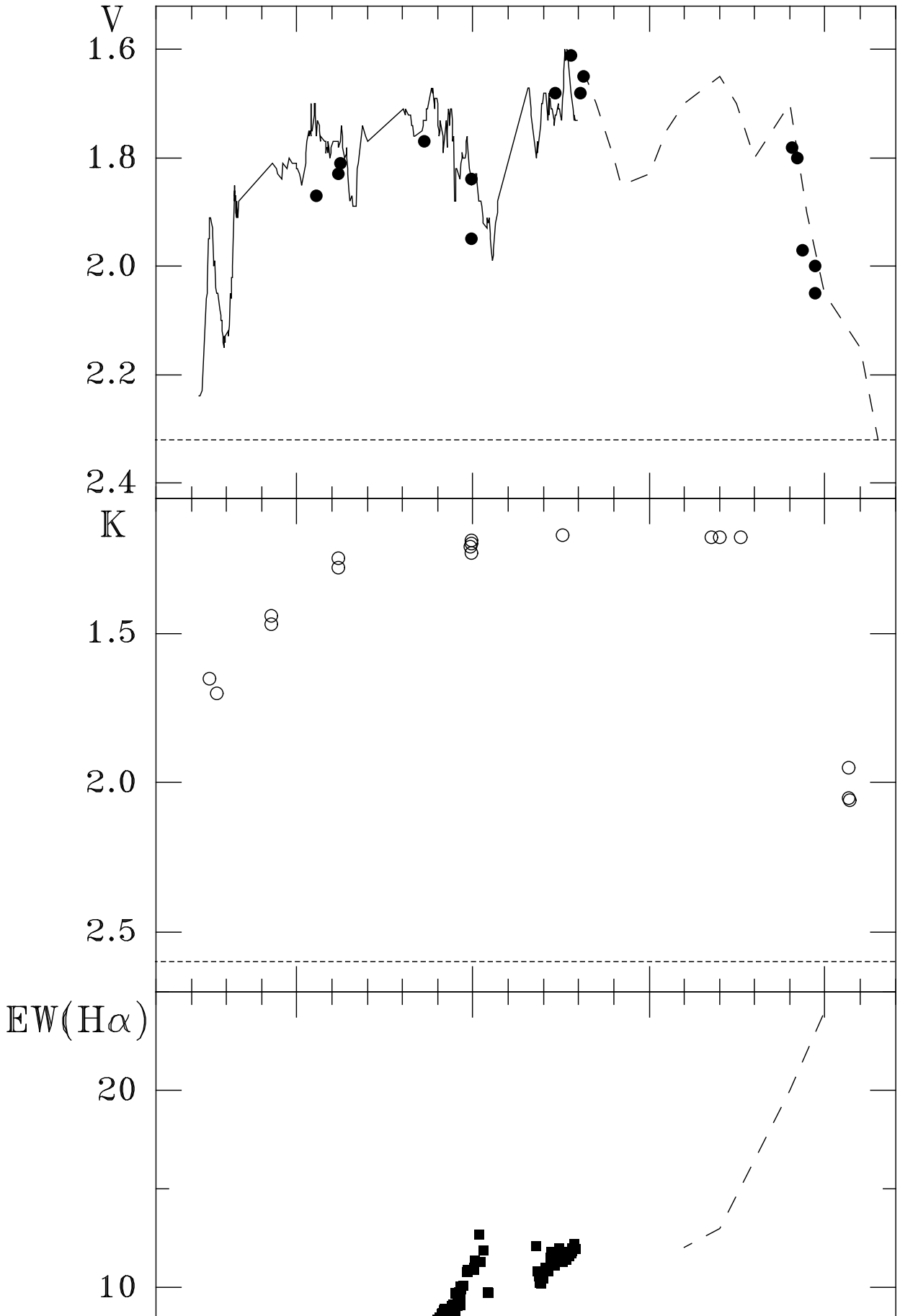
V
1.6
1.8
2.0
2.2
2.4
K
1.5
2.0
2.5
EW(Hα)
20
10

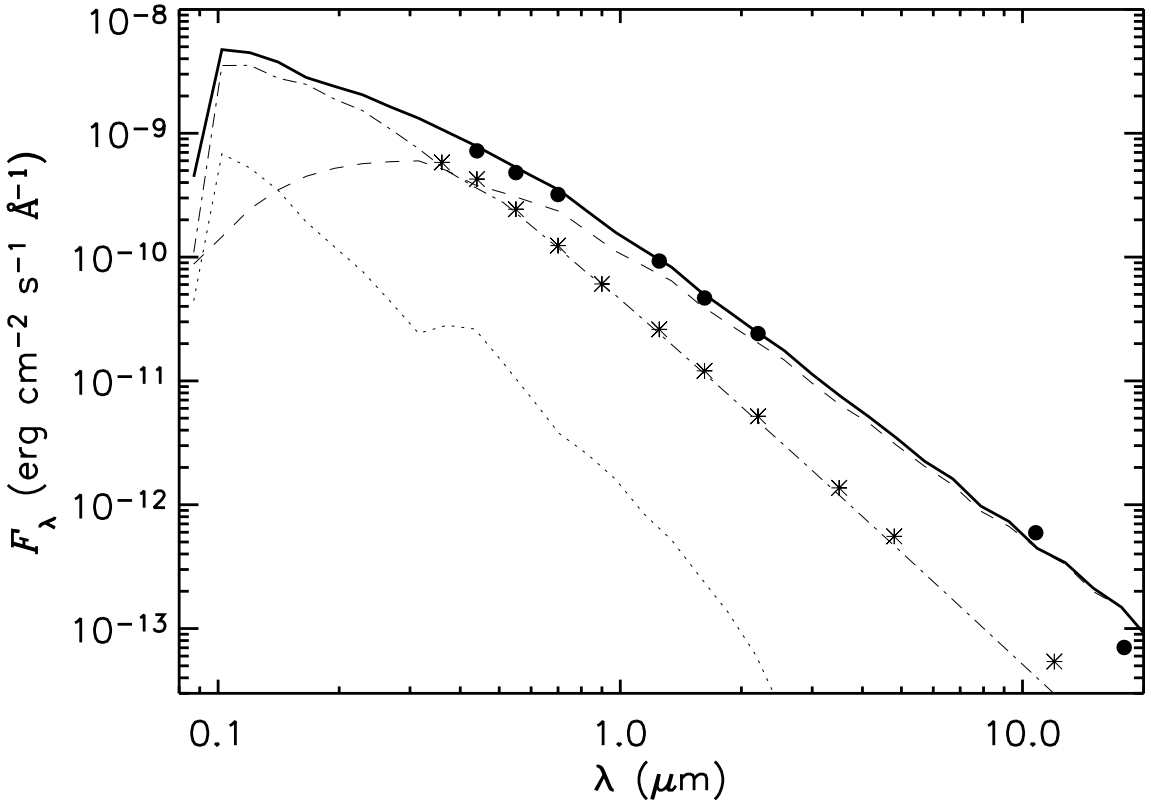

Fig. 2.— Best-fitting model. Our best-fitting SED for the active phase (solid line) is shown along with the observed SED (filled circles). The pre-active phase photometric data taken from the literature also plotted (asterisks) for comparison. The other lines correspond to the scattered, emitted and unprocessed stellar fluxes (dotted, dashed, and dash-dot lines, respectively).

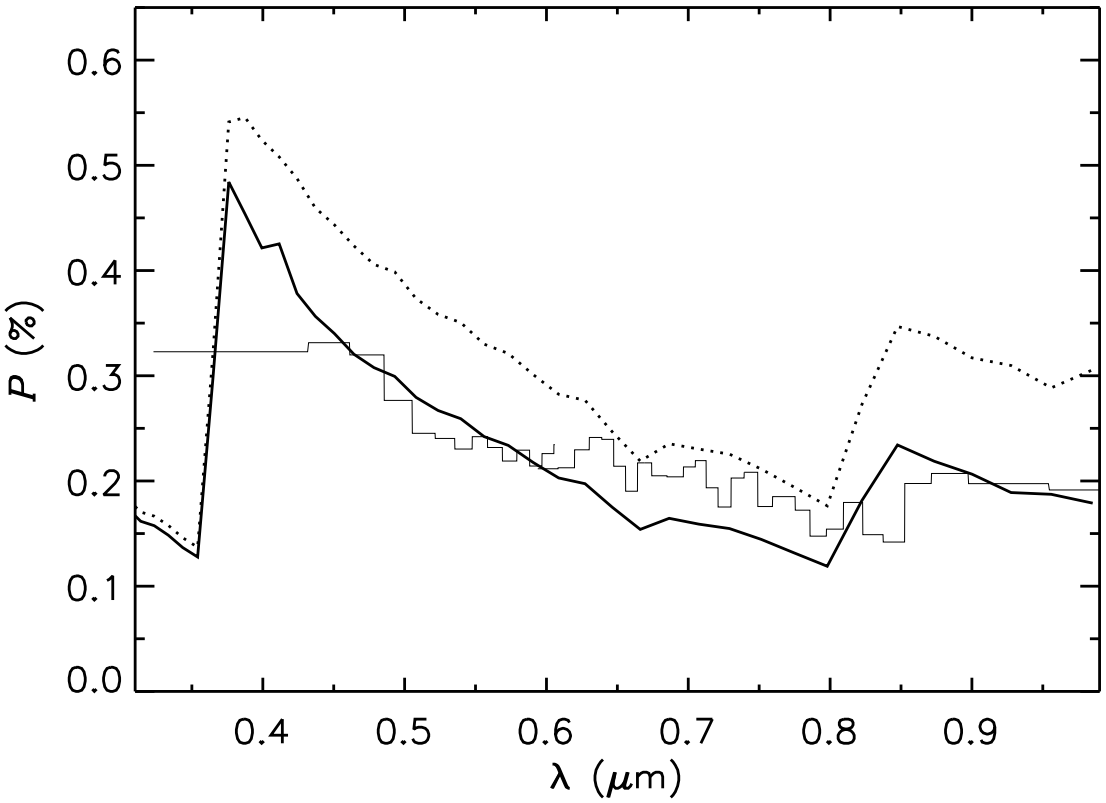

Fig. 3.— Best-fitting model. The best-fitting model polarization (thick line) and the observed polarization (thin line) are shown. The solid thick line correspond to the model polarization with the depolarizing effect of the secondary included, and the dotted thick line correspond to the uncorrected polarization.

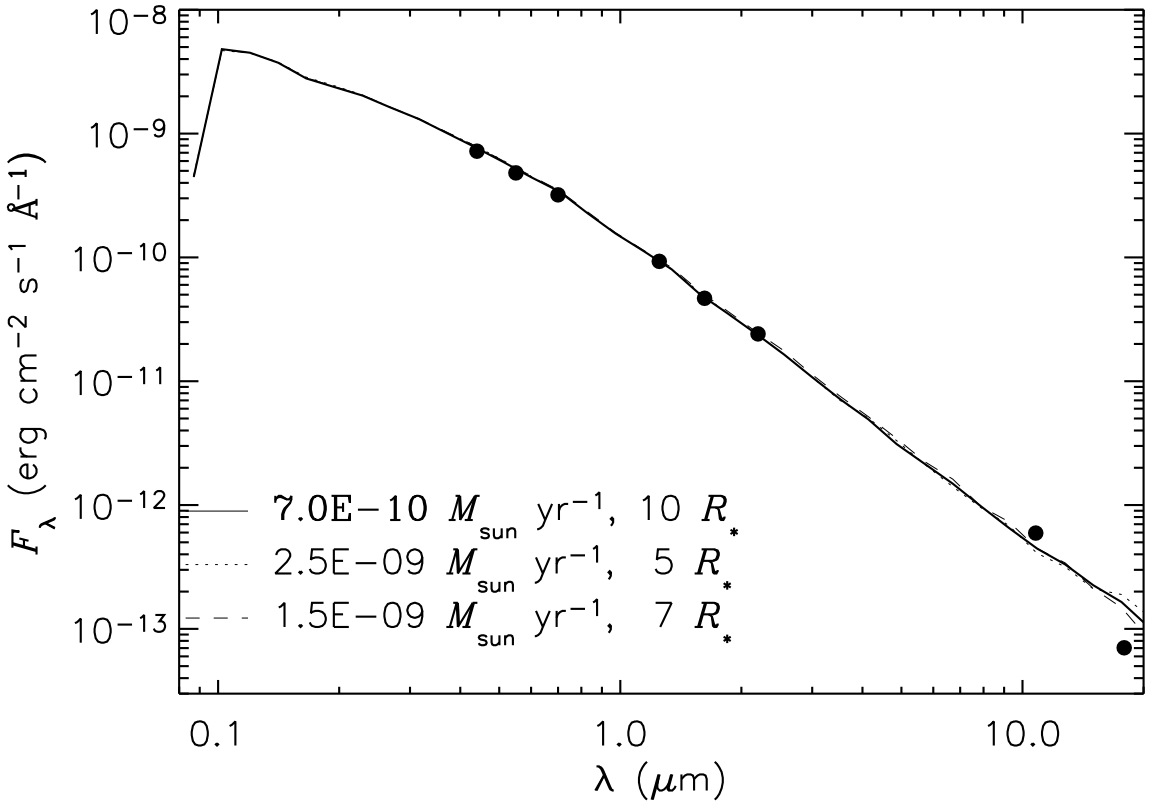

Fig. 4.— Comparison between the SED of different models, as indicated. The circles show the observed active-phase SED.

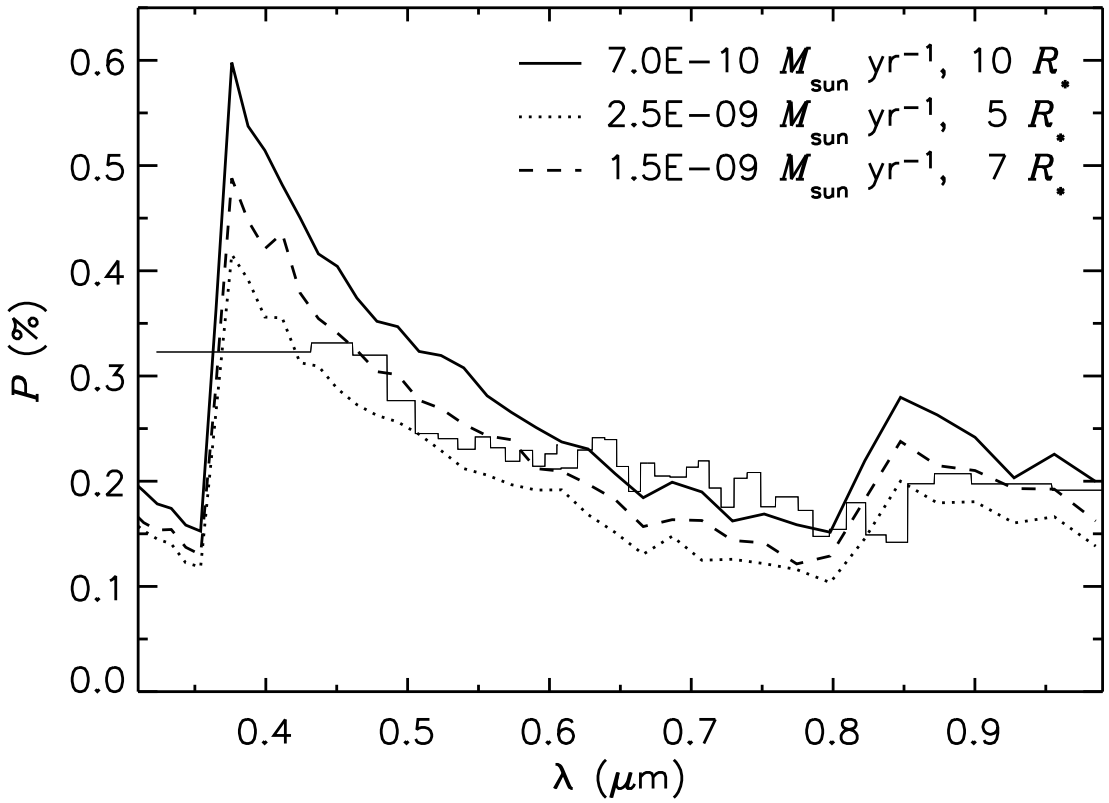

Fig. 5.— Comparison between the polarization of different models, as indicated. The thin line shows the observed polarization.

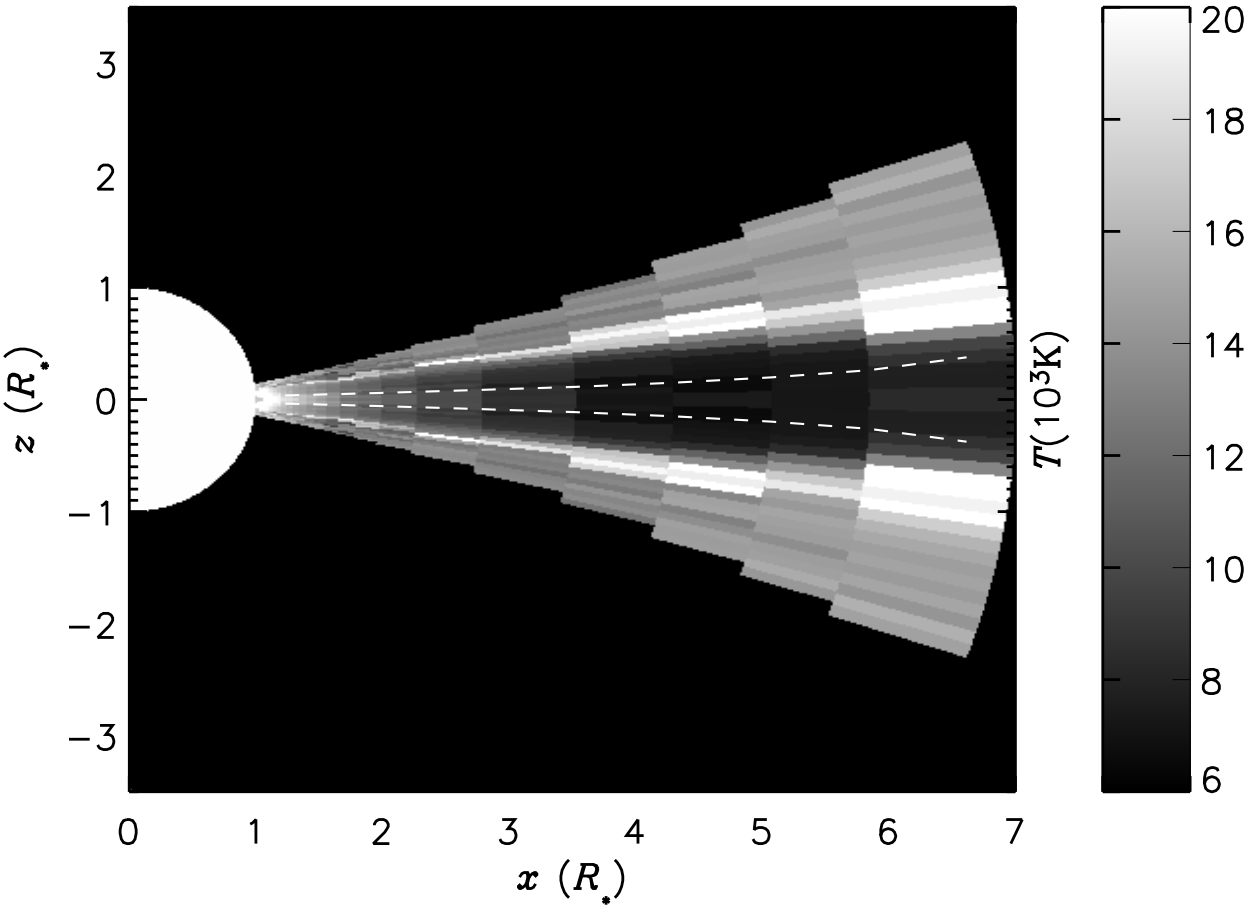

Fig. 6.— Temperature distribution of the best-fitting model. The plot shows the temperature as a function of x and z. The dashed lines correspond to the curves $z = \pm H(x)$ and show that the denser parts of the disk are geometrically very thin.

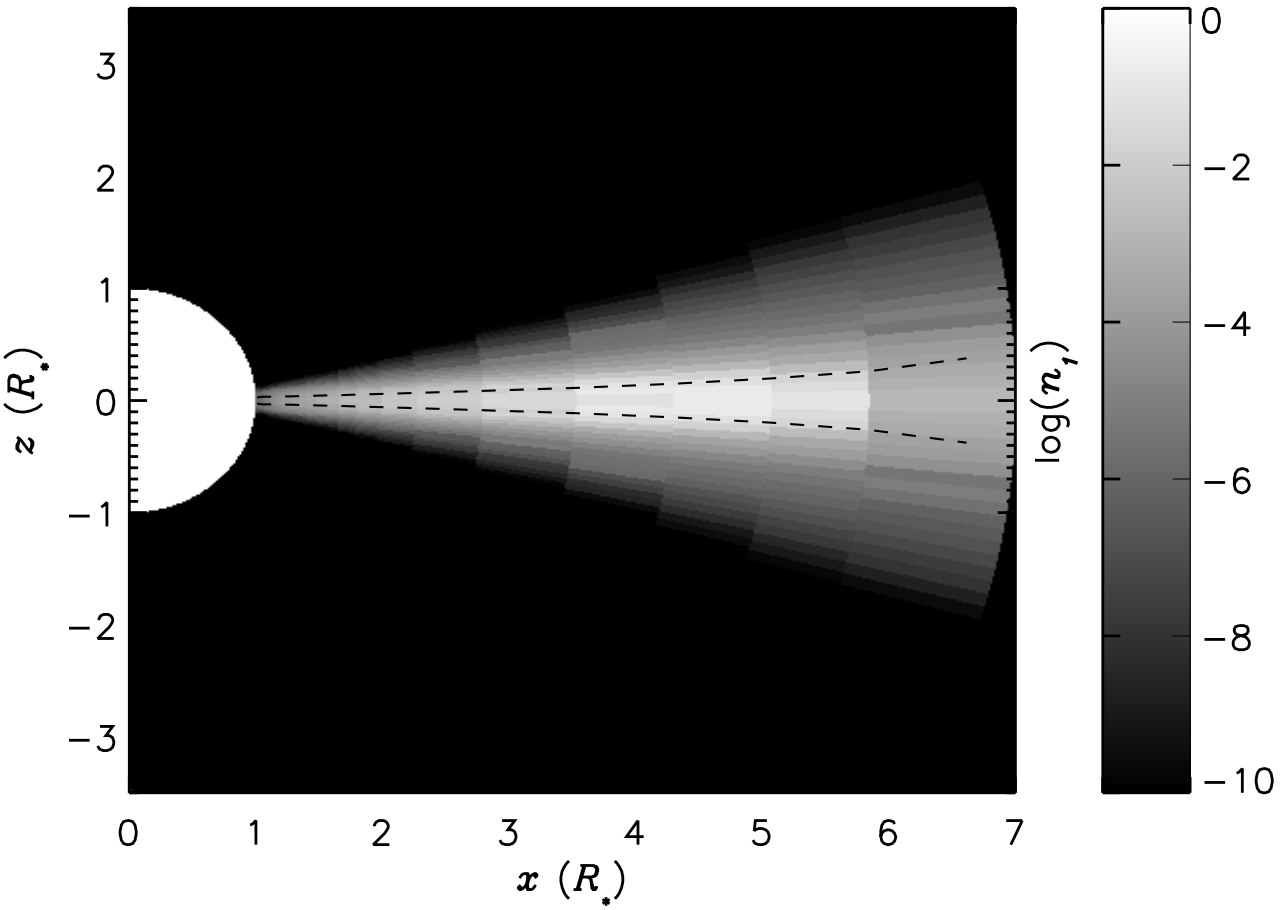

Fig. 7.— $n = 1$ level populations for the best-fitting model. The plot shows the logarithm of the fractional level population as a function of x and z. For a neutral gas, $\log(n_1) = 0$. The dashed lines correspond to the curves $z = \pm H(x)$.

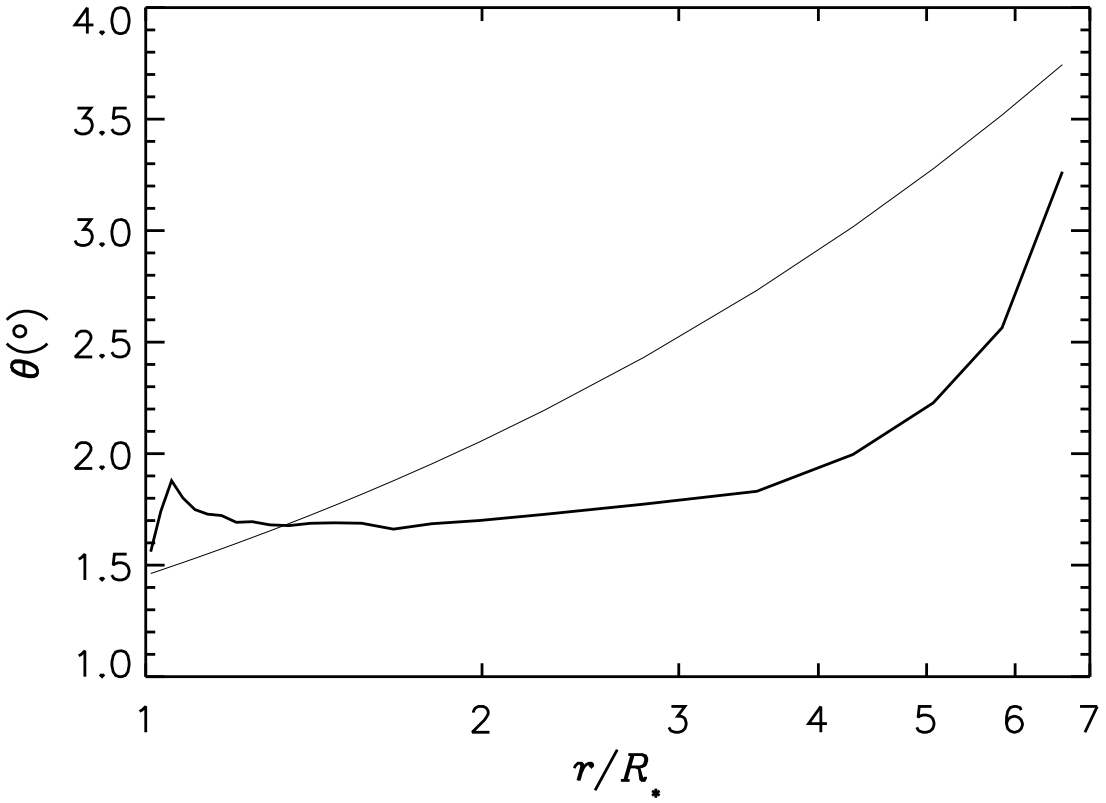

Fig. 8.— Opening angle of the best-fitting model. Shown is the opening angle [thick line, eq. (5)] along with the opening angle of a corresponding isothermal model with $T = 16000$ K (thin line).

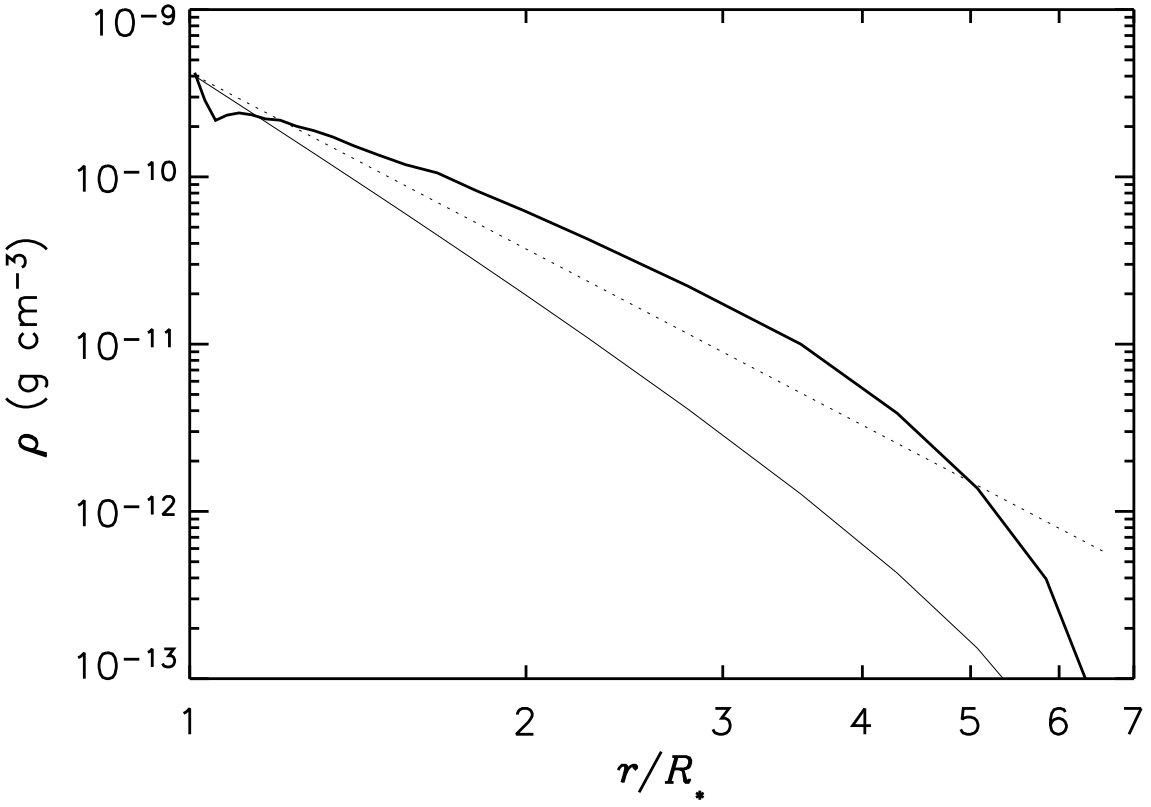

Fig. 9.— Density profile of the best-fitting model. We compare the density calculated from our MC simulation (thick line) to the $\rho \propto \varpi^{-3.5}$ curve expected for an isothermal model (thin line).

Table 1. Optical photometry of δ Sco

MJD	V	$U-B$	$B-V$	$V-R$	$V-I$
2056.27	1.87	–	−0.06	0.12	–
2117.15	1.83	–	0.04	0.27	–
2123.13	1.81	–	0.06	0.23	–
2362.40	1.77	−0.98	0.12	0.24	–
2496.13	1.95	−0.91	0.11	0.24	0.31
2497.14	1.84	−1.02	0.14	–	–
2733.40	1.68	−0.88	0.04	0.20	–
2779.25	1.61	−0.85	0.12	0.29	–
2805.21	1.68	−0.88	0.04	0.24	–
2815.17	1.65	−0.81	0.08	0.33	–
3407.50	1.78	−0.91	0.01	0.19	–
3420.48	1.80	−0.82	0.00	0.17	–
3436.44	1.97	−0.86	−0.02	0.17	–
3471.40	2.00	−0.82	−0.01	0.21	–
3472.36	2.05	−0.86	−0.02	0.16	–

Table 2. Near-IR photometry of δ Sco

MJD	J	H	K	L	Obs.
1751.38	1.77	1.73	1.65	–	Tenerife
1772.38	1.86	1.78	1.70	–	Tenerife
1926.80	1.67	1.58	1.44	–	Tenerife
1927.80	1.66	1.59	1.47	–	Tenerife
2117.41	1.46	1.39	1.25	–	Tenerife
2118.38	1.48	1.41	1.28	–	Tenerife
2492.11	1.53	1.40	–	–	TSAO
2493.11	1.54	1.40	1.21	–	TSAO
2495.10	1.53	1.44	1.20	–	TSAO
2496.13	1.54	–	1.23	–	TSAO
2497.14	1.60	–	1.19	–	TSAO
2753.55	1.45	1.33	1.17	0.90	SAAO
3178.47	1.48	1.35	1.18	0.91	SAAO
3200.38	1.47	1.36	1.18	0.91	SAAO
3262.23	1.48	1.35	1.18	0.87	SAAO
3566.41	2.14	2.07	1.95	–	Tenerife
3567.40	2.19	2.15	2.05	–	Tenerife
3571.42	2.21	2.16	2.06	–	Tenerife

Table 3. Stellar Parameters for δ Sco

$R_\star$ ($R_\odot$)	$T_{\rm eff}$ (K)	$M_\star$ ($M_\odot$)	$V_{\rm crit}$ ($\mathrm{km\,s^{-1}}$)	i (°)	Distance (pc)
7	$27,000$	14	620	38 ± 5	123

Table 4. Best-fit Disk Parameters

$\dot{M}$ ($M_\odot\,\mathrm{yr^{-1}}$)	ρ_0 ($\mathrm{g\,cm^{-3}}$)	R_d ($R_\star$)	i (°)
1.5×10^{-9}	4.5×10^{-10}	7	35